Ultrasound in Med. & Biol., Vol. 39, No. 1, pp. 16–29, 2013

0301-5629/$ - see front matter

ELSEVIER

http://dx.doi.org/10.1016/j.ultrasmedbio.2012.08.004

● *Original Contribution*

REGISTERING PRE- AND POSTRESECTION 3-DIMENSIONAL ULTRASOUND FOR IMPROVED VISUALIZATION OF RESIDUAL BRAIN TUMOR

Laurence Mercier,* David Araujo,* Claire Haegelen,*‡ Rolando F. Del Maestro,†§ Kevin Petrecca,§ and D. Louis Collins*

*McConnell Brain Imaging Centre, Montreal Neurological Institute, McGill University, Montreal, Canada; †Brain Tumour Research Centre, McGill University, Montreal, Canada; ‡INSERM, Faculty of Medicine; INRIA, VisAGeS Unit/Project; CNRS, UMR 6074, IRISA, University of Rennes I, Rennes, France; and §Department of Neurology and Neurosurgery, Montreal Neurological Institute, McGill University, Montreal, Canada

(*Received* 7 *February* 2012; *revised* 8 *August* 2012; *in final form* 10 *August* 2012)

Abstract—The goal of this study was to find a registration technique to improve the alignment of ultrasound images taken before and after brain tumor resection. Validation was performed on 16 tumor cases in 2 ways: (1) manually selected tags on pre- and postresection ultrasounds were used to compute the mean Euclidean distance between corresponding points in the 2 volumes before and after registration; and (2) the surgeon was asked to rank and rate the quality of the alignment before and after registration. The mean distance was 2.7 mm after a rigid registration and 1.7 mm after a nonlinear registration. Of 16 cases, the surgeon determined that initially only 2 were satisfactorily aligned; after the rigid registration, 5 were satisfactory, and after the nonlinear registration, 13 were satisfactory. According to both the distance and the ranking metrics, the nonlinear registration approach significantly improved the alignment of the ultrasound images. (E-mail: louis.collins@mcgill.ca) © **2013 World Federation for Ultrasound in Medicine & Biology.**

Key Words: **Intraoperative ultrasound, Brain tumors, Residual tumor evaluation, Validation, Rigid registration, Nonlinear registration.**

INTRODUCTION

Brain cancer is a challenging disease. For patients with newly diagnosed glioblastoma, the most malignant form of this disease, median survival is less than 18 months (Stupp et al. 2009; Gilbert et al. 2011). Glioblastomas belong to a family of brain tumors called gliomas. When possible, standard treatment of gliomas includes surgical resection, though surgeons unintentionally leave behind some of the tumor more than 50% of the time (Knauth et al. 1999; Unsgaard et al. 2002b; Stummer et al. 2006). This unfortunate reality can be explained by 2 factors. First, most current neuronavigation systems are based on preoperative images, and these systems lose accuracy as the surgery progresses and brain shift increases (Bucholz et al. 1997; Nabavi et al. 2001). Brain shift results from changes in the amount of cerebrospinal fluid (*e.g.*, cyst drainage), gravity, edema, brain tissue resection or retraction, and intracranial pressure management techniques such as the administration of diuretics (*e.g.*, mannitol) (Nimsky et al. 2000; Hartkens et al. 2003). Second, tumor boundaries are often visually and haptically difficult to determine. Because maximum safe resection correlates with longer survival times in patients with both low-grade (Keles et al. 2001; McGirt et al. 2008) and high-grade gliomas (Lacroix et al. 2001; McGirt et al. 2009), the development of intraoperative imaging techniques is desirable because they guide the surgeon toward obtaining a more complete resection while helping to prevent damage to normal brain.

One such technique, intraoperative magnetic resonance imaging (iMRI) (Nimsky et al. 2004; Claus et al. 2005; Hatiboglu et al. 2009), is extremely costly and hence is available in only a few centers. New, much more affordable technologies under development include fluorescence-guided resection (Stummer et al. 2006; Roberts et al. 2011); mass spectrometry (Agar et al. 2011); gamma particle probes (Tipnis et al. 2004; Bonzom et al. 2007; Bogalhas et al. 2009); and tracked

Address correspondence to: D. Louis Collins, PhD., McConnell Brain Imaging Centre, Montreal Neurological Institute, Room WB-314, 3801 University St., Montreal QC H3A 2B4, Canada. E-mail: louis.collins@mcgill.ca

intraoperative 3-dimensional (3D) ultrasound (Unsgaard et al. 2002b; Unsgaard et al. 2005; Tirakotai et al. 2006; Mercier et al. 2011). Fluorescence is useful only for visualizing certain types of tumors and is currently limited to the imaging of surfaces. Mass spectrometry is also limited because it can analyze only *ex vivo* samples, for example, from a biopsy. As for positron emission tomography, patients must be injected with a radioisotope prior to being imaged by a gamma probe (Jerusalem et al. 2003). Ultrasound offers an advantage over iMRI because of its significantly shorter preparation and acquisition times, though it is hindered by a limited field of view and potentially difficult interpretation. In addition, tracked ultrasound costs only a fraction of the price of an iMRI system. Yet very few studies to date have formally compared iMRI and ultrasound: Gerganov et al. (2009) compared ultrasound with high-field iMRI in 26 brain tumor cases and found that image quality before resection was similar in the 2 modalities. Unsgaard et al. (2005) compared 3D ultrasound with preoperative MR images in 28 tumor cases and found that ultrasound was at least as good as MRI for identifying tumor borders. Ultrasound can therefore be used at multiple time points during surgery: (1) at the beginning, to visualize tumor boundaries; (2) during, to update the navigation by compensating for brain shift; and (3) at the end, to evaluate residual tumor and detect hemorrhage beyond the resection borders (Bucholz et al. 1997; Comeau 2000; Unsgaard et al. 2002a; Lunn et al. 2003; Pennec et al. 2003; Rygh et al. 2008; El Beltagy et al. 2010; Mercier et al. 2010a). In contrast to conventional 2-dimensional (2D) ultrasound (Hammoud et al. 1996; Woydt et al. 1996), tracked ultrasound gives a 3D perspective, which allows the surgeon to view the images in more conventional planes (*e.g.*, transverse, coronal, and sagittal) rather than as 2D slices at arbitrary angles. Moreover, the ability to compare ultrasound with preoperative MR images makes tracked ultrasound a more attractive solution for neurosurgeons who are more familiar with MR images than with ultrasound images because it allows simultaneous viewing of the same anatomic cross-section in both ultrasound and MRI.

At our institution, we have developed significant expertise in the use of intraoperative tracked 3D ultrasound. Since 2006, 2 neurosurgeons (R.F.D.M. and K.P.) have been testing tracked ultrasound in a series of adult brain tumor cases (Mercier et al. 2010a; 2010b). In this series, the surgeons always acquired the ultrasound images before starting the resection, in what we call the preresection ultrasound. They then performed the resection and used ultrasound again only at the end of resection, primarily to evaluate residual tumor but also to identify potential undetected bleeding. These postresection ultrasound-produced images, which were often difficult to interpret because their quality was generally lower than that of the preresection images and because a brain shift had occurred, made comparison with earlier images even more difficult. A typical example of pre- and postresection ultrasound images and their initial misalignments is shown in Figure 1. Given this problem, our challenge was to develop a registration technique that would facilitate the localization of residual tumor on the postresection ultrasound. Here we present the first in-depth paper concerning the automatic registration of pre- and postresection 3D B-mode ultrasound images in the context of brain tumor surgery. We explore both rigid and nonlinear registration strategies and validate these techniques in 16 brain tumor cases using 2 different metrics.

Ultrasound

Ultrasound registration poses some specific challenges. As Gee et al. (2004) noted, "Unlike other modalities, differences in the two volumes might be due to different directions of insonification, or different time-gain-compensation settings on the ultrasound machine, and not due to real anatomical changes." In addition, important anatomic changes occur between the acquisitions, both in terms of resected tissue and in shifts in the surrounding anatomy. The presence of Surgicel (Ethicon, Somerville, NJ), a surgical hemostat composed of

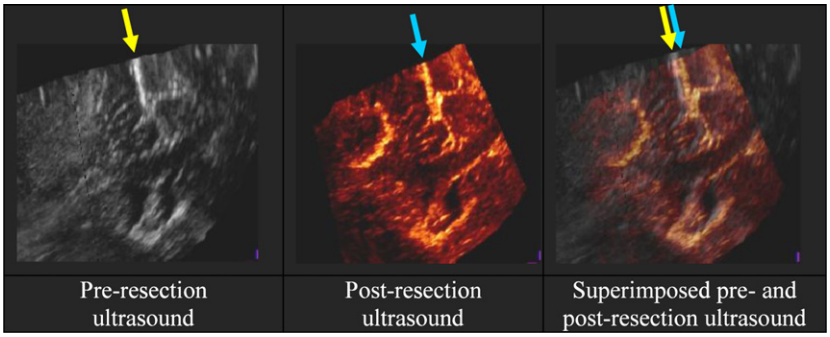

Fig. 1. Preresection *(gray shades)* and postresection *(warm shades)* ultrasound images. *Arrows* indicate the falx and show its misalignment in images taken at different time points *(far right)*.

oxidized cellulose, can also create major artifacts in the postresection ultrasound (Fig. 2). In our study, 50% (8/16) of the postresection ultrasounds were performed with Surgicel in the resection cavity, which created a hyperechoic artifact that degraded the quality of the images.

Most of the literature concerning ultrasound and ultrasound registration has focused on acquisitions taken at the same time point for spatial compounding. Spatial compounding is meant to reduce certain image artifacts by imaging the same area from slightly different angles and has been tested with rigid body (Rohling et al. 1997, 1998), affine (Shekhar and Zagrodsky 2002), and nonlinear registration (Krucker et al. 2000; Xiao et al. 2002). Gee et al. (2003) used rigid-body registration for larger-field-of-view ultrasound and found that the choice of similarity criteria was not critical. Nonrigid ultrasound–ultrasound registration has also been used in the case of ultrasound taken on the skin to correct for the varying pressures of the probe (Treece et al. 2002). Using the concept of attribute vectors, Foroughi et al. (2006) elastically registered 3D ultrasound images of the liver at the same time point but with different applied deformations.

Few articles have been published about the registration of ultrasound images taken at different time points with known changes in the underlying anatomy, though some work has been done in cardiac (Shekhar and Zagrodsky 2002; Shekhar et al. 2004) and breast imaging (Moskalik et al. 1995). For example, Narayanasamy et al. (2009) temporally registered separated acquisitions of the breast to monitor tumor size following chemotherapy. For registration, they used the MIAMI Fuse software developed at the University of Michigan (Ann Arbor, MI), first with a full-affine registration, followed by a nonrigid thin-plate spline registration. In neurosurgery, Pennec et al. (2003) imaged both a simple phantom made of 2 balloons and a dead pig brain and performed nonrigid ultrasound-ultrasound image–based registrations to compensate for the deformations. In the same year, Letteboer et al. (2003a; 2005) published studies on rigid and nonrigid (Letteboer et al. 2003b) registration of 1 ultrasound sweep taken on the dura and another taken just after the dura was opened. A few authors have used Doppler images for ultrasound–ultrasound registration: Meyer et al. (1999) with breast images, Porter et al. (1999) with liver images and, finally, our group (Reinertsen et al. 2007) with brain images. However, to our knowledge, no one has attempted to register B-mode ultrasound images taken before and at the end of neurosurgery.

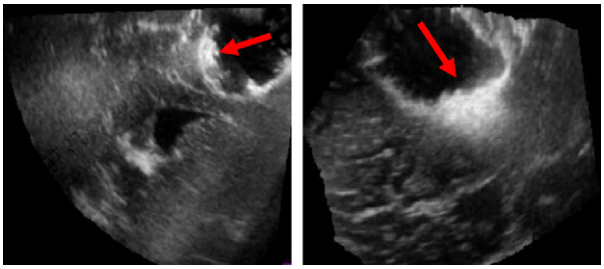

Fig. 2. Ultrasound image showing artifact caused by the presence of Surgicel in the resection cavity.

MATERIALS AND METHODS

Equipment

Images were acquired using our prototype neuronavigation system, IBIS (Mercier et al. 2011). IBIS consists of a computer (dual-core Intel Xeon 3 GHz processor (IBM, Armonk, NY) running Debian GNU-Linux 3.1) connected to an ultrasound machine (HDI 5000, ATL/Philips, Bothell, WA) and a tracking device. The ultrasound probe was a P7-4 MHz phased array transducer at depth settings of 6.5 cm and 8 cm and was tracked by reflective spheres rigidly fixed to a TA003 tracker (Traxtal Technologies, Toronto, ON, Canada) by a Polaris infrared optical system (Northern Digital, Waterloo, ON, Canada). Because the probe cannot be sterilized, it is draped in a plastic sleeve, through which the sterile spheres are clipped. To calibrate the probe, a phantom with 4 Z-fiducials was used (Gobbi et al. 1999). Ultrasound images were transferred to the computer by a Pinnacle PCTV frame-grabbing card (Pinnacle Systems, Mountain View, CA).

Patients

The 16 patients with brain tumors (7 females, 9 males; mean age, 51 years) included in this study are detailed in Table 1. The patients all had suspected gliomas based on their preoperative MR images. After histologic examination, it was determined that 4 patients had low-grade gliomas, 11 had high-grade gliomas, and 1 patient had a dysembryoplastic neuroepithelial tumor. All tumors were supratentorial and located in various lobes. Mean tumor volume was 30 cm^3, ranging from 0.2 cm^3 to 79.2 cm^3. Half of the cases were first operations, and half were reoperations. To decrease intracranial pressure and facilitate surgery, all patients were hyperventilated and given mannitol prior to craniotomy. All patients provided informed consent. The study was approved by the Montreal Neurological Institute and Hospital Review Ethics Board.

Imaging protocols

All patients included in the study underwent a preoperative MRI examination on a 1.5 Tesla GE Signa EXCITE (General Electric, Milwaukee, WI). The preoperative images were transferred to the IBIS station and

Table 1. The 16 tumor cases included in the study

Case number	Sex	Age	Tumor type	Tumor location	Tumor volume (cm^3)	Operation redo	Location of postresection US
1	f	59	LGG	Left frontal	17.6	Redo	Dura
2	m	55	HGG	Left temporal	10.9	Redo	Dura
3	f	25	DNT	Left temporal	3.4	First	Cavity
4	f	42	HGG	Left frontal	63.1	Redo	Dura
5	m	31	LGG	Right frontal	79.2	First	Dura
6	m	70	HGG	Left parietotemporal	53.7	First	Dura
7	m	72	HGG	Right parietal	31.6	First	Dura
8	m	39	HGG	Left frontal	0.2*	Redo	Dura
9	m	40	HGG	Left frontal	32.3	Redo	Cavity
10	m	62	HGG	Left temporal	13.9	Redo	Dura
11	f	42	HGG	Left frontal	4.8	First	Cavity
12	f	49	HGG	Left frontal	10.4	Redo	Dura
13	f	40	LGG	Right frontal	39.7	First	Dura
14	f	72	HGG	Left frontal	49.1	First	Dura
15	m	76	HGG	Right parietal	31.9	Redo	Dura
16	m	70	LGG	Right temporal	37.7	First	Dura
Means		51			30.0		

DNT = dysembryoplastic neuroepithelial tumor; HGL = high-grade glioma; LLG = low-grade glioma; US = ultrasound.
* This tumor was accompanied by a massive cyst.

converted from Digital Imaging and Communications in Medicine (DICOM) to Medical Imaging NetCDF (MINC) format (Neelin 1998). In the operating room, a standard patient registration procedure using 9 facial landmarks was performed to allow conventional navigation and planning based on the preoperative MR images (Wolfsberger et al. 2002).

Ultrasound images were acquired before and after tumor resection. Preresection ultrasound was preferably acquired on the dura, though dural acquisition was possible only in first operations or if the dura was used to close the cavity from a previous surgery. Otherwise, images were taken either directly on the cortex (or tumor) or on a dural repair patch (Dura-Guard, Synovis Surgical Innovations, St. Paul, MN) applied to the cortex. The surgeon then visualized the tumor and surrounding anatomy on both the intraoperative ultrasound and the preoperative MR images to identify any differences. After this first ultrasound, the surgeon resected the tumor until what he thought was the maximum possible resection. The postresection ultrasound was used to verify the cavity to detect any residual tumor or hemorrhage. Whenever possible, this ultrasound was acquired inside the resection cavity. Sometimes, however, the orientation of the surgical cavity was in the shape of a C rather than a U and could therefore not contain the saline necessary for ultrasound imaging. In these cases, the cavity was closed with Dura-Guard, which would retain the saline for imaging. For the postresection ultrasound in this study, when both the in-cavity and on-dura images were available, the ultrasound image volume with the largest overlap with the preresection ultrasound was chosen. The on-dura postresection image generally overlapped the on-dura preresection image better, which is why it was chosen most often (see last column of Table 1). Because they generally covered more of the tumor bed than the in-cavity images, the on-dura images may also be considered more clinically relevant.

Ultrasound image processing

Once acquired, the 2D ultrasound images were reconstructed in a 3D volume using a pixel-based method (Solberg et al. 2007). Each pixel from each tracked 2D image was reconstructed onto a regular 3D grid using linear interpolation and an isotropic regrid radius of 0.3 mm. Beyond the 0.3 mm radius, if no pixel covered a given voxel, the voxel was set to zero. The resulting gaps are masked out during the registration process. Typically, sweeps contained between 200 and 600 frames of 2D ultrasound data and were reconstructed at a voxel size of $0.3 \times 0.3 \times 0.3$ mm^3. All images were converted to the MINC format (Neelin 1998), the format used at our institute for image processing. Processing was performed with various publicly available MINC tools (packages.bic.mni.mcgill.ca) on the IBIS station.

Improving the initial alignment of images

In the operating room, all images are transformed into the world space, which is the coordinate system defined by the tracking device. Preoperative MR images are transformed into world space by patient registration. Ultrasound images are transformed into world space by concatenating the ultrasound probe calibration and the pose of the tracker fixed on the probe. In a previous publication (Mercier et al. 2011), the point reconstruction accuracy of our calibration was estimated to be in the 0.49 to 0.74 mm range. If all these transformations were exact and no brain shift had occurred, the preoperative MR images and pre- and postresection ultrasound images would all be perfectly aligned. Instead, we found

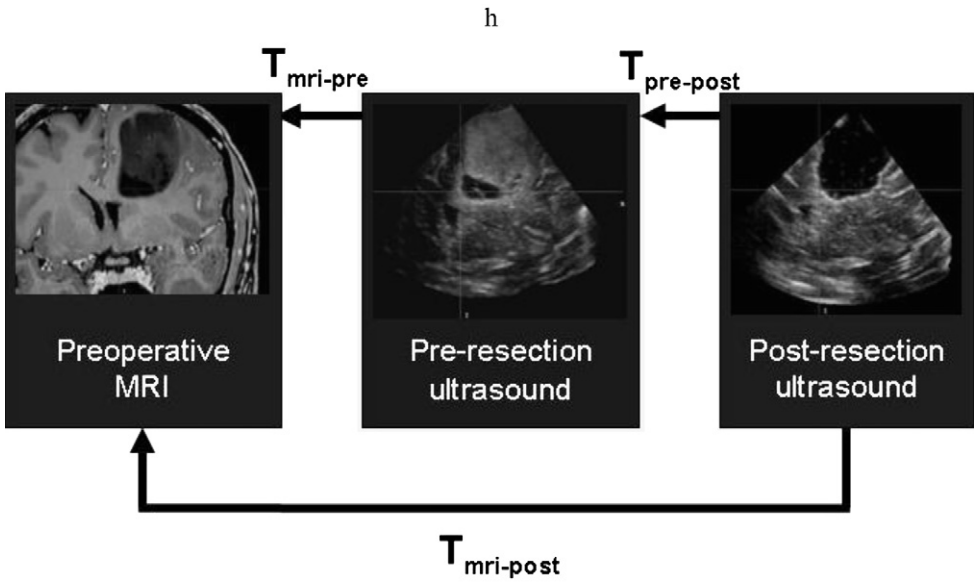

Fig. 3. The varying transformations *(T)* between the preoperative MR images and intraoperative ultrasound images. The transformation can be nonlinear or rigid. The subscript should be read from right to left in the same manner as matrix multiplications are carried out.

misalignment of various magnitudes among images. We found that improving the alignment of these 3 images helped the surgeon compare the different image volumes—and made the ultrasound more useful because it enabled the combination of complementary information given by each image volume.

Figure 3 shows the necessary alignment corrections (or transformations) among the images, where $T_{mri\text{-}pre}$ is the transformation between the preresection ultrasound and the preoperative MR images. Previous publications by our group (Mercier et al. 2010a, 2012) showed that our pseudo-ultrasound approach was robust and successful in registering preresection ultrasound and preoperative MR images. Using a series of corresponding anatomic landmarks chosen by 2 experts from 15 pairs of MR and ultrasound images, the mean residual distance between the 2 images was significantly improved from an initial 5.34 mm to 2.97 mm after registering with the pseudo-ultrasound technique. The pseudo-ultrasound basically transforms the MR image into an ultrasound-like image to facilitate registration. Figure 4 shows an example of an MR image transformed into a pseudo-ultrasound image. We tried to use this registration approach to estimate $T_{mri\text{-}post}$ with the postresection ultrasound, though unsuccessfully; the technique may have to be adapted to cope with the resection cavity. Instead, we opted for a simpler approach: registering the pre- and postresection ultrasounds, basically optimizing $T_{pre\text{-}post}$. To transform the postresection ultrasound into the preoperative MR image space, we simply need to concatenate the 2 transformations, $T_{pre\text{-}post}$ and $T_{mri\text{-}pre}$.

Proposed registration techniques

Registration of the pre- and postresection ultrasound images was performed with a MINC tool called minctracc. A large series of minctracc options and input

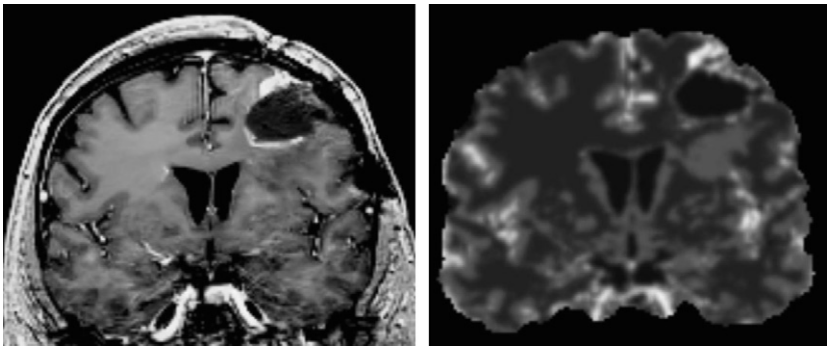

Fig. 4. Left: MR image of the head. Right: Corresponding pseudo-ultrasound of the brain.

preprocessing were tested iteratively, and the best rigid body and nonlinear registration parameters were chosen. For the rigid registration approach, we tested cross-correlation, mutual information, and normalized mutual information (NMI). Based on a visual alignment assessment and distance measurements using a bronze standard (described in the next subsection), it was determined that NMI gave the best results and is therefore reported here. For the nonlinear approach, the only 2 objective functions currently implemented in minctracc are the cross-correlation and the normalized correlation coefficient, and they are very similar. Although the correlation coefficient should be less sensitive to overall intensity differences among the images, the 2 functions gave almost identical results. We report the results obtained with the correlation coefficient objective function because they were slightly better. Note that the nonlinear registration uses the rigid-body registration as initialization. The algorithm then builds up a 3D nonlinear deformation field in a piecewise linear fashion. The deformable registration method can be described by the following equation: $T(x) = A(x) + D(A(x))$, where A is an affine transformation and D is a field of deformations vectors. Cubic splines are used to interpolate the deformation for any arbitrary point. While the ANIMAL technique (Collins and Evans 1997) used here is not theoretically diffeomorphic (*i.e.*, continuous and invertible), the constraints imposed on it make it continuous and numerically invertible. Table 2 summarizes the inputs and parameters used with minctracc for this study.

For the input images, we tested various types of preprocessing, mainly blurring and median-filtering the images with various kernels, again using the distance measurements of a bronze standard. Surprisingly, for the rigid registration, the original images gave the best results, possibly because the 3D reconstruction algorithm we used had already smoothed the data. For the nonlinear registration, a Gaussian kernel with a 2 mm full width at half maximum performed best. Blurring images often helps in smoothing the cost function, which leads to fewer problems with local minima. For both the linear and nonlinear techniques, the registration was improved when using the preresection ultrasound images as sources and the postresection ultrasound images as targets.

The purpose of the ultrasound mask is to exclude the black background that contains no data. The background comes from the reconstruction stage in which the 2D ultrasound images are masked to remove all annotations from the original image. The mask also included the gaps (if any) in the 3D images. This masking step is crucial for the success of the registration, because the edges and the gaps could otherwise be considered as strong false-edges, which could make the registration less robust. As Table 2 indicates, we used the same mask for both the rigid and nonlinear registrations (the intersections between the masks of the pre- and postresection ultrasound volumes). For repeatability purposes, the exact minctracc parameters used for the rigid and nonlinear methods, respectively, were:

minctracc –identity –step 1 1 1 – simplex 0.5 –nmi –lsq6 –speckle 0 pre-us.mnc post-us.mnc –source mask pre-us-mask.mnc –model_mask post-us-mask.mnc

and

minctracc -nonlinear corrcoef –step 2 2 2 –transform linear.xfm -simplex 1 –weight 1 –similarity 0.3 – max 30 –iter 20– lattice_diameter 6 6 6 – sub_lattice 6 –stiff 1.

These parameters were identified by iterative trials. When gaps were present, the data on each side of the gap were interpolated to create a continuous nonlinear deformation field.

Registration validation with manual tags

No gold standard for evaluation is available for clinical data, so our ultrasound–ultrasound alignment bronze standard (Jannin et al. 2002) was defined by selecting corresponding anatomic landmarks in the ultrasound images. For each of the 16 cases, a neuroradiologist (D.A.) chose 10 corresponding anatomic features. The homologous landmark points were chosen using the MINC tool register. For landmark points, we could use any anatomic structures visible on ultrasound, such as sulci bifurcations, vessels, choroid plexus, foramens, septa, and so forth. Choosing 10 points generally took 30 to 45 min per case. The mean distance between the corresponding points enables a quantitative estimation of the accuracy of the alignment between the ultrasound volumes. The mean distance was computed as the mean absolute Euclidean distance between the corresponding points in the 2 ultrasound images.

Because it is very time consuming, the point-picking process was done over a period of several months. To evaluate the intraobserver variability in point selection,

Table 2. Inputs and parameters for registration with minctracc

Method	Objective function	Source	Target	Source mask	Target mask
Rigid	NMI	Original preresection ultrasound	Original postresection ultrasound	Intersection mask	Intersection mask
Nonlinear	Correlation coefficient	Blurred preresection ultrasound	Blurred postresection ultrasound	Intersection mask	Intersection mask

NMI = normalized mutual information.

points for 3 cases were selected a second time. The cases were divided into 3 groups, determined by the date on which they were selected, and the median of the group was chosen for reselecting. Note that the selecting was not done in chronologic order. Following that convention, the 3 following cases were chosen for reselecting: 4, 10, and 13. For these cases, we kept the same points on the preresection ultrasound but chose the corresponding points again on the postresection ultrasound.

Registration evaluation by neurosurgeon

The quality of the alignment of the pre- and postresection ultrasounds was also visually assessed by a neurosurgeon (C.H.). This aspect is important because, in the operating room, it is the surgeon who decides whether the alignment of the 2 modalities is adequate. Visual ratings were obtained to determine the number of cases for which a realignment was necessary to be able to extract the information from the postresection ultrasound. For each of the 16 tumor cases, the surgeon was simultaneously presented with 3 pairs of images. The postresection ultrasound was constant and was superimposed on (1) the original preresection ultrasound; (2) the preresection ultrasound after a rigid correction; and (3) the preresection ultrasound after a nonlinear correction. To avoid any bias, the images were assigned random names so that the surgeon would be blind to which pair corresponded to what category. The surgeon first had to rank the images from 1 to 3, with 1 corresponding to the best registration. Then a binary score was assigned to each pair: 1, if the images were sufficiently aligned for residual tumor evaluation; and 0, if the surgeon would have to request a realignment.

RESULTS

Precision of point selecting on ultrasound

The anatomic landmarks chosen to evaluate the registration results must be accurate. In the 3 cases used to evaluate intraobserver variability, the mean distance between homologous landmarks in the tag-retag experiment was 1.58 ± 1.2 mm (mean ± standard deviation). Table 3 shows the mean distance for each of the 3 cases.

To evaluate the effect of landmarking on the variability of the distance measurement, the 2 sets of tags on the postresection volume were used, and the preresection landmarks were used to estimate the difference in mean distance between the pre- and postresection ultrasounds. Table 4 shows the mean distance between the preresection tag set and the first and second tag sets chosen on the postresection ultrasound. The mean difference between the 2 sets of tags for these 3 cases was 0.27 mm.

Table 3. Reproducibility results: mean Euclidean distance between the 2 tag sets selected on the postresection ultrasound for 3 cases

Patient number	Mean distance (mm)
4	1.70
10	2.11
13	0.92

Registration accuracy

Tables 5 and 6 summarize the registration accuracy results on a case-by-case basis. In terms of the mean distances computed with the tags (Table 5), the ultrasound images were at an initial distance of 3.3 mm (range, 1.0 to 10.5 mm). This distance was reduced to 2.7 mm (0.9 to 6.4 mm) after a rigid correction and 1.7 (0.7 to 3.7 mm) after a nonlinear correction. According to the visual rankings (Table 6), the nonlinear alignment was ranked number 1 (best) in 14 of the 16 cases. In the 2 cases where the nonlinear alignment did not yield the best result, the residual misalignments were very small to start with (1 and 1.5 mm), and were even smaller quantitatively after nonlinear registration (0.9 and 1.1 mm), but qualitatively the linear transformation was preferred for the first case, and the initial transformation was preferred for the second case.

In Table 6, the green cells indicate the cases that were sufficiently aligned according to the surgeon's visual assessment, and the red cells indicate those that were not. These color-coded cells show that, according to the surgeon's visual assessment, 14 of 16 cases from the initial pre- and postresection ultrasound alignment needed improvement. After a rigid correction, 11 cases required further alignment improvements. After applying the proposed nonlinear correction to all 16 pairs, 13 cases were considered sufficiently aligned and only 3 still needed improvement.

To determine whether the mean distances in columns 2, 3, and 4 in Table 5 were statistically different, a repeated measures analysis of variance (ANOVA) was applied. This yielded $F(2,30) = 8.5$, $p = .0012$, indicating that the differences were significant. A post hoc Tukey test showed no difference between the initial and rigid

Table 4. Reproducibility results: mean Euclidean distance between the pre- and postresection ultrasounds for 3 cases as evaluated using 2 different sets of tags

Patient number	Mean distance using first tag set (mm)	Mean distance using second tag set (mm)	Difference (mm)
4	2.71	2.60	0.11
10	4.42	3.87	0.55
13	2.88	2.74	0.14
Mean difference for the 3 patients			0.27

Table 5. Results

Patient number	Initial*	Results after rigid correction	Results after nonlinear correction
1	1.0 (0.5–1.8)	1.3 (0.8–2.1)	0.9 (0.5–1.5)
2	1.5 (0.5–3.3)	1.8 (0.8–4.1)	1.1 (0.4–3.5)
3	2.1 (1.1–2.8)	1.7 (0.9–2.9)	1.3 (0.8–1.9)
4	2.7 (1.7–4.1)	1.8 (0.7–3.2)	1.4 (0.5–3.2)
5	2.3 (0.6–5.4)	3.1 (1.0–5.7)	1.3 (0.2–3.7)
6	3.9 (2.8–5.1)	1.6 (0.4–3.1)	1.0 (0.5–1.9)
7	4.6 (3.0–5.9)	6.3 (4.8–8.0)	3.7 (0.9–6.6)
8	4.1 (2.6–5.5)	1.5 (0.5–2.8)	1.3 (0.5–2.8)
9	2.3 (1.4–3.1)	1.0 (0.2–2.3)	1.1 (0.5–1.6)
10	4.4 (3.0–5.4)	2.4 (0.3–4.2)	2.2 (1.1–4.8)
11	2.2 (1.0–4.6)	5.3 (3.6–7.9)	1.4 (0.3–3.9)
12	3.9 (0.98–6.7)	3.7 (2.2–4.7)	2.9 (0.92–5.8)
13	2.9 (0.76–9.0)	2.8 (0.67–8.3)	2.2 (0.23–9.5)
14	10.5 (7.8–13.0)	6.4 (3.9–9.4)	3.7 (0.37–9.3)
15	1.6 (1.3–2.2)	0.9 (0.60–1.6)	0.7 (0.35–2.0)
16	2.2 (0.60–4.0)	1.8 (0.20–3.3)	1.4 (0.47–4.4)
Grand mean	3.3	2.7	1.7

Note: Each cell contains the mean Euclidean distance (mm) between the 10 tag sets and the range.

* Results of the pre- and postresection ultrasounds in their initial positions.

transformations, but there was a statistically significant improvement between the rigid and nonlinear transformations ($p < .05$) and between the initial and nonlinear transformations ($p < .01$).

A nonparametric Friedman test was used to check for statistical differences between the qualitative rankings of the various registrations in Table 6. This yielded a $\chi^2(2) = 17.38$, $p < .0001$, indicating that the rankings were indeed different. A post hoc 2-by-2 Wilcoxon test

Table 6. Results

Patient number	Initial*	Results after rigid correction	Results after nonlinear correction
1	2	1	3
2	1	3	2
3	3	2	1
4	3	2	1
5	2	3	1
6	3	2	1
7	3	2	1
8	3	2	1
9	3	2	1
10	3	2	1
11	3	2	1
12	3	2	1
13	2	3	1
14	3	2	1
15	3	2	1
16	2	3	1
Mean	3.2	2.7	1.7

Note: The number in each cell represents the visual ranking by the surgeon (from 1 to 3). The cell color is a binary score: green indicates that the surgeon thought the alignment was adequate; red indicates that a realignment would be necessary.

* Results for the pre- and postresection ultrasounds in their initial positions.

Table 7. Summary of statistical results

	Initial/ rigid	Rigid/ nonlinear	Initial/ nonlinear
Distances (Tukey)	Non significant	$p < .05$	$p < .01$
Rankings (Wilcoxon)	Non significant	$p < .04$	$p < .01$

Note: The methods agree on the significance of each comparison.

of the ranks yielded no significant differences between the initial and the rigid transformations. There was, however, a statistically significant improvement between the rigid and nonlinear transformations ($p < .04$) and between the initial and nonlinear transformations ($p < .01$). Table 7 summarizes the statistical results.

DISCUSSION

Quality of landmarks

Comparing different registration methods requires objective accuracy metrics. On clinical images, because no gold standard is available, manually identified landmarks are often used as a bronze standard (Jannin et al. 2002). Here, Table 3 shows that the intraobserver variability was 1.58 mm, indicating accurate and reliable manual identification of landmarks. Table 4 shows that the variability in measuring registration quality was 0.27 mm, which is good considering the 0.3 × 0.3 × 0.3 mm voxel size. Measures repeated more than twice and in more than 3 cases would have been a better bronze standard.

Brain shift estimation

The mean distance estimates in the second column of Table 5 can be used to estimate brain shift occurring between the pre- and postresection ultrasounds. Figure 5 gives a visual example of the magnitude of brain shift for case number 4. The largest brain shift in this example is located on the left side of the falx where the tumor is, as expected. The mean shift in this series of 16 patients with brain tumor is 3.2 mm, which may seem low when compared with the numbers often reported in the literature concerning brain shift. Not all reports, however, use the same metric to quantify brain shift. Many studies measure brain shift at the surface of the cortex only, often with the goal of using the deformation at the surface to drive a biomechanical model (Miga et al. 1999; Roberts et al. 1999) to deform the rest of the brain. In our study, the points were chosen at least 1 cm below the surface, mostly in deeper areas of the brain, in regions neighboring the tumor. As Hastreiter et al. (2004) demonstrated, shifts at the surface and of deeper brain structures may be uncorrelated. Therefore, our discussion concentrates on studies reporting only nonsurface brain shift measurements.

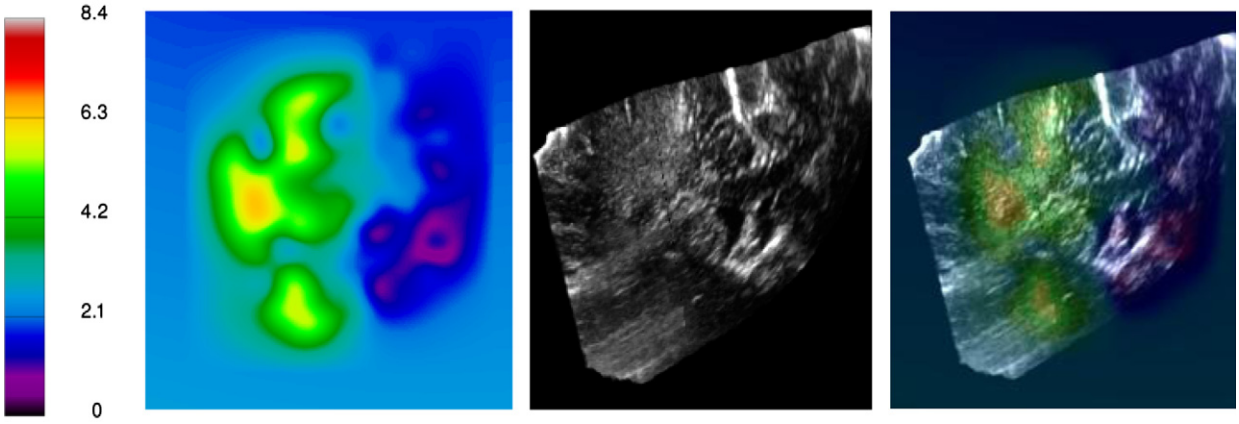

Fig. 5. 2D color map showing the magnitude of brain shift (in mm) as computed after rigid and nonlinear registrations of the pre- and postresection ultrasound images for patient #4 (left). The value outside the ultrasound image region is not 0 because of the rigid registration. Preresection ultrasound (center). The 2 previous images combined (right).

Brain shift estimation using tracked pointer

Two often-cited papers, Hill et al. (1998) and Roberts et al. (1998), feature in-depth studies of brain shift, yet their measurements are limited to quantifying the displacement of the cortical surface. As for brain shift below the surface, Dorward et al. (1998) used a tracked pointer to compare the position of certain structures with the preoperative MR image. Their measurements were made on 48 tumor cases, 18 of which were gliomas, the tumor type studied in our report. For gliomas, they found a mean shift of 3.5 mm at the deep tumor margin after dural opening (but before resection). The problem with using a tracked pointer is the possible overestimation of brain shift because it includes the patient–MR image registration error. Thus, Dorward et al. (1998) were actually measuring the target registration error rather than brain shift alone. For more accurate estimation, brain shift, ideally, should be measured by the same modality at 2 different time points during surgery.

Brain shift estimation using intraoperative magnetic resonance imaging

Several groups have used intraoperative MRI to study brain shift (Maurer Jr. et al. 1998; Nabavi et al. 2001; Hartkens et al. 2003; Trantakis et al. 2003; Hastreiter et al. 2004; Clatz et al. 2005). In one of the most in-depth papers, Nabavi et al. (2001) imaged 25 patients with supratentorial tumors in an open-bore 0.5T scanner but, again, measurements were taken on the cortical surface only.

Hastreiter et al. (2004) evaluated brain shift in 2D in a series of 32 gliomas using a 0.2T iMRI system. They found maximum deep tumor margin shifts ranging from −7.9 mm to 30.9 mm and from 2.3 mm to 4.0 mm in the midline.

Hartkens et al. (2003) estimated brain shift in 3D by performing nonlinear registration of pre- and postresection MR images in 13 brain tumor cases. The results are reported in a graph, with ipsilateral and contralateral results presented separately. Because the ultrasound images and tags were acquired almost exclusively ipsilateral to the tumor, we compared our findings with only those results. From their graph, we computed a mean brain shift ipsilateral to a tumor of 5.5 mm, which is slightly higher than our findings.

In a series of 8 tumor cases, Hill et al. (1998) used mutual information to do a linear followed by a nonlinear registration of pre- and postresection MR images. They measured shifts using both manually selected points and the magnitude of the deformation throughout the head. Results were separated into ipsilateral and contralateral; we compared our results only with the ipsilateral numbers (their Table 3). They found slightly higher shift with the manual points versus the deformation field (1.5 mm *vs.* 1.3 mm). These brain shift numbers seem low, but it must be remembered that they chose points in many lobes, sometimes far from the tumor. If we look at the lobe with the maximum shift for each patient and compute the mean for each category, we get 3.0 mm for the manual points and 2.6 mm for the overall deformation field, which is very similar to our findings.

Brain shift estimation using tracked ultrasound

Brain shift studies using tracked ultrasound are rare (Keles et al. 2003; Letteboer et al. 2005) and, again, include primarily displacement at the surface. The 2 studies referenced here have nonsurface measurements but measured brain shift in 2 dimensions only. Bucholz et al. (1997) measured brain shift at 3 time points: (1) after the opening of the skull (termed preresection);

(2) after the opening of the dura mater (opened dura); and (3) after the removal of the lesion (postresection). Brain shift was measured by comparing manually selected points on the 2D ultrasound and resliced MR image (or computed tomography). Their study included 23 neurosurgeries, 15 of which were for brain tumor and had an average 2D postresection shift of 7.3 ± 5.8 mm. Their measurements were made on a variety of internal structures, such as ventricles, tumor, sulci, blood vessels, choroid plexus, and so forth. They found that the magnitude of the brain shift was much higher in structures like sulci and blood vessels than in landmarks near the falx. As in Dorward et al. (1998), these brain shift measures also include the patient–MRI registration error.

Keles et al. (2003) estimated the shift between pre- and postresection ultrasounds in 13 brain tumor cases and found a mean shift of 2 mm, which is even lower than our results. They found no shift in 2 of the 13 patients (15%). Only patients with expected large shifts were included in the study, so we can hypothesize that the brain shift estimates in that study would have been even lower in an unselected sample.

Comparison of brain shift numbers

Compared with our findings, Hartkens et al. (2003) found slightly higher brain shift estimates using intraoperative MRI (5.5 mm *vs.* 3.2 mm) possibly because, as mentioned earlier, ultrasound does not image the cortical surface, where the largest deformations occur. Second, to obtain an image at the end of resection, the resection cavity must be filled with saline, which prevents the surrounding tissue from collapsing. It is unclear whether, in studies using MRI, the cavity was filled before imaging. If it was, susceptibility artifacts would be reduced; if not, it could explain why postresection brain shift measurements are larger when measured by MRI than by ultrasound.

Adding quadrature to our previous estimate of MRI-preresection ultrasound misregistration (5.3 mm (Mercier et al. 2012)) with the brain shift found here (3.2 mm) yields 6.2 mm, a result comparable to the 7.3 mm reported by Bucholz et al. (1997).

Although we expected a larger mean brain shift, when compared with the results of similar studies, our findings appear to be consistent with the literature. The way our tags were selected could, however, slightly underestimate brain shift. In our series of data, the largest shifts were generally seen in the immediate vicinity of the tumor (<1 cm) and in the lateral ventricles. Each case contains points in the ventricular region, but the immediate vicinity was occasionally hard to capture. In some cases, the sulci had become much larger and changed shape, making an exact match impossible; hence, we chose points slightly farther away, where corresponding points could be chosen with more certainty.

Registration issues

Our results indicate that even if the brain shift is relatively small, in the vast majority of cases, the surgeon still needs a correction to the alignment of the postresection ultrasound to compare it with the preresection images. As reported by Hill et al. (1998), when registering pre- and postresection MR images, linear registration does not seem to be sufficient to align properly the pre- and postresection ultrasounds. The nonlinear registration technique proposed here has the advantages of being extremely simple to implement and of being robust. According to the surgeons' ratings, however, it is not yet perfect; 3 cases still needed a larger correction. Perhaps more complex approaches such as those used in a similar context for MRI–MRI registration (Clatz et al. 2005; Archip et al. 2007; Ding et al. 2009; Risholm et al. 2009; Chitphakdithai and Duncan 2010; Yixun et al. 2010) would further improve the registration results.

Concerning ultrasound–ultrasound registration, Gee et al. (2003) found that the choice of objective function was not critical. Letteboer et al. (2003a) and Ijaz et al. (2010) found that NMI gave the best results, which is what we found here with the rigid-body registration.

Using nonlinear registration, we were able to improve the ultrasound image alignment from a mean of 3.2 mm to 1.7 mm, an improvement of 1.5 mm. This is the same as the point-picking precision obtained in our reproducibility tests (1.58 mm). We have demonstrated, however, that the improvement was indeed statistically significant with the surgeons' rankings and ratings, which gave almost exactly the same results as the distance measurements.

Timing issues

In terms of timing, the rigid registration method described in this article takes about 1 min to perform, and the resampling of the ultrasound image, about 10 s. The nonlinear registration takes about 3 min, and the associated resampling, 4 min. These calculations were done prospectively, and no effort was made to optimize the timing issue; hence, it could certainly be improved. At our institution, a glioma surgery generally takes about 7 to 8 hours, so waiting about 10 min (3D reconstruction + rigid registration + nonlinear registration + resampling) would be acceptable. Considering that cleaning the cavity and acquiring ultrasound images takes at most 10 min, we are still below the 20-min mark, which is well below what would be necessary to acquire a postresection intraoperative MRI in most centers.

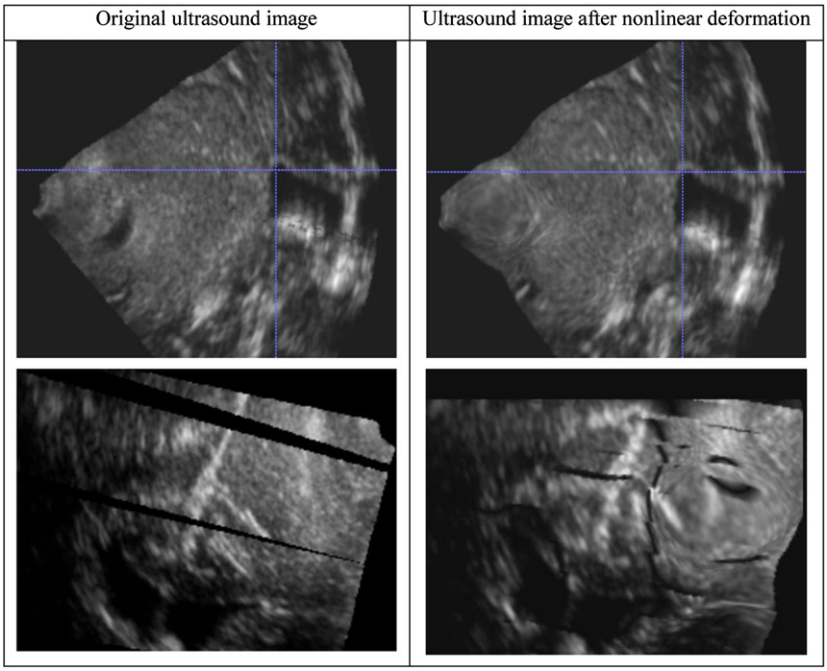

Fig. 6. Examples of artifacts caused by nonlinear deformation of ultrasound images. Original ultrasound image (left). After nonlinear resampling (right).

Resampling issues

When visually examining the deformed ultrasound images with the surgeons, we realized that resampling ultrasound images that have large nonlinear deformations can create some visually problematic artifacts. One problem comes from the speckle in the ultrasound images; it is the result of a random, deterministic interference pattern coming from subresolution scatterers in the tissue. After a nonlinear deformation the speckle, which usually appears as a textured pattern, can sometimes be transformed into little curve segments. This phenomenon can be observed in the upper right image in Figure 6, where the deformed speckle has formed 3 artificial circles in the left part of the image. One possible way to improve this situation would be to deform ultrasound images with less speckle, like a median-filtered or denoised ultrasound (de Fontes et al. 2011).

We do not fill the holes in the 3D ultrasound reconstruction when some 2D images are missing because we do not want to create "artificial tissue," which would be interpolated from the surrounding voxels. In our series, 2 cases had rather large gaps, as in the second row in Figure 6. Generally, such gaps are caused by the probe's being out of view of the tracking camera for about 1 s. Deforming images with such gaps creates artifacts, as in Figure 6.

Visualization aspects

Clearly, a nonlinear registration is necessary in order to compare pre- and postresection images. With the resampling issues presented in the previous subsection, one may ask whether resampling the postresection ultrasound is the best choice in terms of visualization. The clinical standpoint must also be considered. The following paragraph summarizes the various options for the optimal visualization and localization of residual tumor based on postoperative ultrasound.

The preresection ultrasound is already linearly registered to the preoperative MRI, so should these 2 images be nonlinearly warped to look like the postresection ultrasound? From an engineer's point of view, this would seem to be the most logical course of action because the postresection ultrasound shows the current state of the brain. The 3 neurosurgeons involved in this study had a different perspective: the preoperative MRI was their reference, the basis of their entire plan for the surgery. Therefore, it makes more sense to warp the postresection ultrasound to the preoperative MRI. However, this approach could be problematic in cases with large brain shifts. On ultrasound, a thin ($\sim$2 to 3 mm) hyperintense rim around the cavity usually means no residual tumor. Because the brain has a tendency to move back into place as the tumor is resected, the surgical cavity is generally smaller than the original tumor. As a result, if the cavity is significantly warped to fit a larger tumor, some sections of the thin rim might become larger, which could potentially pose a problem for interpretation because it could resemble residual tumor. The surgeon would therefore need both the initial and the warped postresection ultrasound. That way, the surgeon could look at the rim before any nonlinear deformation occurred.

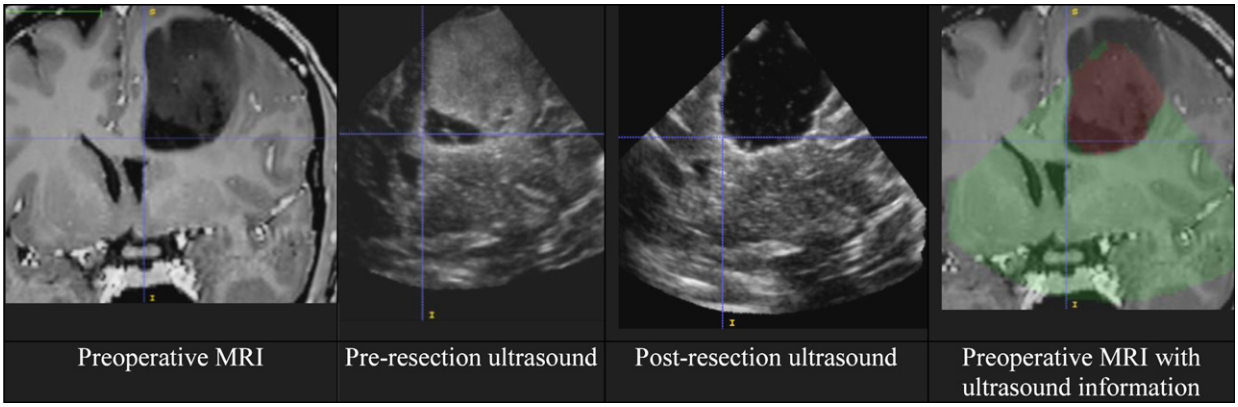

Fig. 7. Images that could be presented to the surgeon at the end of resection. From left to right: preoperative MR image; rigidly registered preresection ultrasound; rigidly registered postresection ultrasound; preoperative MR image with overlaid nonlinearly warped resection cavity *(red)*; and the region covered by the postresection ultrasound *(green)*.

In our series, we also found it difficult to interpret the postresection ultrasound because its quality was generally lower than that of the preresection image. One way of taking advantage of the warped postresection ultrasound and making that information easy for the surgeon to understand would be to extract the resection cavity and map that information onto the preoperative MRI. Figure 7 is a series of images that could be presented to the surgeon at the end of resection.

Another way to make the postresection ultrasound easier to interpret would be to have a tool to guide the surgeon during the image acquisition that would make sure that the 3D volume has no gaps. A technique to fill the remaining gaps, if any, could also be used, but we prefer an approach in which no "false data" are added. To better identify the gaps in the deformed ultrasound, the gaps could simply be identified using a color other than black, like red or green, for example.

Clinical issues

The goal of our study was not to evaluate the clinical validity of the registration method, but one might wonder about the potential clinical impact of the proposed registration process on surgery and whether it warrants the extra time and workflow disruption it would cause. Based on our experience with a limited number of cases, we hypothesize that improved registration of the pre- and postresection ultrasound images makes it easier for the surgeon to evaluate the presence and location of residual tumor and thus easier to decide whether further resection is needed. If our process does indeed improve the amount of resected tumor, we believe the extra time involved is justified.

CONCLUSIONS

For a surgeon, determining the borders of a glioma is often challenging, but intraoperative imaging can help to achieve a more complete resection. Surgeons find it easier to interpret postresection ultrasounds when they are properly aligned with preresection images. Our findings show that a simple nonlinear correlation coefficient registration significantly improves the alignment between pre- and postresection ultrasound images from a mean distance of 3.2 mm to 1.7 mm. Although experiments have shown that nonlinearly deforming an ultrasound can make it more difficult to interpret, we have suggested techniques that register, resample, and clearly present the images to the surgeon so as to help improve the resection.

Acknowledgments—This work was financed by the *Fonds québécois de la recherche sur la nature et les technologies*; Canadian Institutes of Health Research (MOP-97820); Natural Science and Engineering Research Council of Canada; Franco Di Giovanni Foundation; B-Strong, Alex Pavanel family; Raymonde and Tony Boeckh Fund; Montreal English School Board; Brainstorm Foundation; Tony Colannino Foundation; and Brain Tumor Foundation of Canada. Dr. R. F. Del Maestro holds the William Feindel Chair in Neuro-Oncology at McGill University. We thank Dr. Vladimir Fonov for all of his technical help.

REFERENCES

Agar NY, Golby AJ, Ligon KL, Norton I, Mohan V, Wiseman JM, Tannenbaum A, Jolesz FA. Development of stereotactic mass spectrometry for brain tumor surgery. Neurosurgery 2011;68:280–290.

Archip N, Clatz O, Whalen S, Kacher D, Fedorov A, Kot A, Chrisochoides N, Jolesz F, Golby A, Black PM, Warfield SK. Non-rigid alignment of pre-operative MRI, fMRI, and DT-MRI with intra-operative MRI for enhanced visualization and navigation in image-guided neurosurgery. Neuroimage 2007;35:609–624.

Bogalhas F, Charon Y, Duval MA, Lefebvre F, Palfi S. Development of a positron probe for localization and excision of brain tumours during surgery. Physics Med Biol 2009;54:443–449.

Bonzom S, Menard L, Pitre S, Duval MA, Siebert R, Palfi S, Pinot L, Lefebvre F, Charon Y. An intraoperative beta probe dedicated to glioma surgery: Design and feasibility study. Nucl Sci IEEE Trans 2007;54:30–41.

Bucholz RD, Yeh DD, Trobaugh JW, McDurmott LL. The correction of stereotactic inaccuracy caused by brain shift using an intraoperative ultrasound device. Lecture Notes in Computer Science 1997;1205: 459–466.

Chitphakdithai N, Duncan J. Non-rigid registration with missing correspondences in preoperative and postresection brain images. In: Jiang T, Navab N, Pluim J, Viergever M, (eds). Medical Image

Computing and Computer-Assisted Intervention. Berlin/Heidelberg: Springer; 2010. p. 367–374.
Clatz O, Delingette H, Talos IF, Golby AJ, Kikinis R, Jolesz FA, Ayache N, Warfield SK. Robust nonrigid registration to capture brain shift from intraoperative MRI. IEEE Trans Med Imaging 2005;24:1417–1427.
Claus EB, Horlacher A, Hsu L, Schwartz RB, Dello-Iacono D, Talos F, Jolesz FA, Black PM. Survival rates in patients with low-grade glioma after intraoperative magnetic resonance image guidance. Cancer 2005;103:1227–1233.
Collins DL, Evans AC. Animal: Validation and applications of nonlinear registration-based segmentation. Int J Patt Recogn A I 1997;11: 1271–1294.
Comeau R. Intraoperative Ultrasound Imaging for the Detection and Correction of Tissue Movement in Image-guided Neurosurgery. Department of Biomedical Engineering. Montreal, McGill University. PhD. 2000.
de Fontes FP, Barroso GA, Coupé P, Hellier P. Real time ultrasound image denoising. J Real-Time Image Proc 2011;6:15–22.
Ding S, Miga MI, Noble JH, Cao A, Dumpuri P, Thompson RC, Dawant BM. Semiautomatic registration of pre- and post brain tumor resection laser range data: method and validation. IEEE Trans Biomed Eng 2009;56:770–780.
Dorward NL, Alberti O, Velani B, Gerritsen FA, Harkness WF, Kitchen ND, Thomas DG. Postimaging brain distortion: Magnitude, correlates, and impact on neuronavigation. J Neurosurg 1998;88: 656–662.
El Beltagy M, Aggag M, Kamal M. Role of intraoperative ultrasound in resection of pediatric brain tumors. Childs Nerv Sys 2010;26: 1189–1193.
Foroughi P, Abolmaesumi P, Hashtrudi-Zaad K. Intra-subject elastic registration of 3D ultrasound images. Med Image Anal 2006;10: 713–725.
Gee A, Prager R, Treece G, Cash C, Berman L. Processing and visualizing three-dimensional ultrasound data. Br J Radiol 2004;77-2: S186–S193.
Gee AH, Treece GM, Prager RW, Cash CJ, Berman L. Rapid registration for wide field of view freehand three-dimensional ultrasound. IEEE Trans Med Imaging 2003;22:1344–1357.
Gerganov VM, Samii A, Akbarian A, Stieglitz L, Samii M, Fahlbusch R. Reliability of intraoperative high-resolution 2D ultrasound as an alternative to high-field strength MR imaging for tumor resection control: A prospective comparative study. J Neurosurg 2009;111: 512–519.
Gilbert MR, Wang B, et al. RTOG 0525: A randomized phase III trial comparing standard adjuvant temozolomide (TMZ) with a dose-dense (dd) schedule in newly diagnosed glioblastoma (GBM). American Society of Clinical Oncology (ASCO) Annual Meeting, Chicago, 2011.
Hammoud MA, Ligon BL, elSouki R, Shi WM, Schomer DF, Sawaya R. Use of intraoperative ultrasound for localizing tumors and determining the extent of resection: A comparative study with magnetic resonance imaging. J Neurosurg 1996;84:737–741.
Hartkens T, Hill DL, Castellano-Smith AD, Hawkes DJ, Maurer CR Jr, Martin AJ, Hall WA, Liu H, Truwit CL. Measurement and analysis of brain deformation during neurosurgery. IEEE Trans Med Imaging 2003;22:82–92.
Hastreiter P, Rezk-Salama C, Soza G, Bauer M, Greiner G, Fahlbusch R, Ganslandt O, Nimsky C. Strategies for brain shift evaluation. Med Image Anal 2004;8:447–464.
Hatiboglu MA, Weinberg JS, Suki D, Rao G, Prabhu SS, Shah K, Jackson E, Sawaya R. Impact of intraoperative high-field magnetic resonance imaging guidance on glioma surgery: A prospective volumetric analysis. Neurosurgery 2009;64:1073–1081.
Hill DL, Maurer CR Jr, Maciunas RJ, Barwise JA, Fitzpatrick JM, Wang MY. Measurement of intraoperative brain surface deformation under a craniotomy. Neurosurgery 1998;43:514–526. discussion 27–28.
Ijaz UZ, Prager RW, Gee AH, Treece GM. Optimization strategies for ultrasound volume registration. Meas Sci Technol 2010;21:085803.
Jannin P, Fitzpatrick JM, Hawkes DJ, Pennec X, Shahidi R, Vannier MW. Validation of medical image processing in image-guided therapy. IEEE Trans Med Imaging 2002;21:1445–1449.
Jerusalem G, Hustinx R, Beguin Y, Fillet G. PET scan imaging in oncology. Eur J Cancer 2003;39:1525–1534.
Keles GE, Lamborn KR, Berger MS. Low-grade hemispheric gliomas in adults: A critical review of extent of resection as a factor influencing outcome. J Neurosurg 2001;95:735–745.
Keles GE, Lamborn KR, Berger MS. Coregistration accuracy and detection of brain shift using intraoperative sononavigation during resection of hemispheric tumors. Neurosurgery 2003;53:556–562. discussion 62–64.
Knauth M, Wirtz CR, Tronnier VM, Aras N, Kunze S, Sartor K. Intraoperative MR imaging increases the extent of tumor resection in patients with high-grade gliomas. Am J Neuroradiol 1999;20: 1642–1646.
Krucker JF, Meyer CR, LeCarpentier GL, Fowlkes JB, Carson PL. 3D spatial compounding of ultrasound images using image-based nonrigid registration. Ultrasound Med Biol 2000;26: 1475–1488.
Lacroix M, Abi-Said D, Fourney DR, Gokaslan ZL, Shi W, DeMonte F, Lang FF, McCutcheon IE, Hassenbusch SJ, Holland E, Hess K, Michael C, Miller D, Sawaya R. A multivariate analysis of 416 patients with glioblastoma multiforme: Prognosis, extent of resection, and survival. J Neurosurg 2001;95:190–198.
Letteboer MM, Willems PW, Viergever MA, Niessen WJ. Brain shift estimation in image-guided neurosurgery using 3-D ultrasound. IEEE Trans Biomed Eng 2005;52:268–276.
Letteboer MMJ, Viergever MA, Niessen WJ. Rigid registration of 3D ultrasound data of brain tumours. Computer Assisted Radiology and Surgery 2003a;1256:433–439.
Letteboer MMJ, Willems PWA, Viergever MA, Niessen WJ. Non-rigid registration of 3D ultrasound images of brain tumours acquired during neurosurgery. In: Ellis RE, Peters TM, (eds). Medical image computing and computer-assisted intervention: MICCAI 2003. Heidelberg, Germany: Springer Berlin; 2003b. p. 408–415.
Lunn KE, Paulsen KD, Roberts DW, Kennedy FE, Hartov A, West JD. Displacement estimation with co-registered ultrasound for image guided neurosurgery: A quantitative in vivo porcine study. IEEE Trans Med Imaging 2003;22:1358–1368.
Maurer CR Jr, Hill DLG, Martin AJ, Liu H, McCue M, Rueckert D, Lloret D, Hall WA, Maxwell RE, Hawkes DJ, Truwit CL. Investigation of intraoperative brain deformation using a 1.5T interventional MR system: Preliminary results. IEEE Trans Med Imaging 1998;17: 817–825.
McGirt M, Chaichana K, Attenello F, Weingart J, Than K, Burger P, Olivi A, Brem H, Quinoñes-Hinojosa A. Extent of surgical resection is independently associated with survival in patients with hemispheric infiltrating low-grade gliomas. Neurosurgery 2008;63: 700–707.
McGirt M, Chaichana K, Gathinji M, Attenello F, Than K, Olivi A, Weingart J, Brem H, Quiñones-Hinojosa AR. Independent association of extent of resection with survival in patients with malignant brain astrocytoma. J Neurosurg 2009;110:156–162.
Mercier L, Del Maestro RF, et al. Experience using intraoperative 3D ultrasound in 14 brain tumors cases. Canadian Neuro-Oncology Meeting, Niagara-on-the-Lake, Canada, 2010a.
Mercier L, Del Maestro RF, et al. Experience using intraoperative 3D ultrasound in conjunction with preoperative MRI in brain tumor surgery. 5th Annual Scientific Meeting of the Society for Neuro-Oncology, Montreal, Canada, 2010b.
Mercier L, Del Maestro RF, Petrecca K, Kochanowska A, Drouin S, Yan CXB, Janke AL, Chen SJ-S, Collins DL. New prototype neuronavigation system based on preoperative imaging and intraoperative freehand ultrasound: System description and validation. Int J Comput Assist Radiol Surg 2011;6:507–522.
Mercier L, Fonov V, Haegelen C, Del Maestro R, Petrecca K, Collins DL. Comparing two approaches to rigid registration of three-dimensional ultrasound and magnetic resonance images for neurosurgery. Int J Comput Assist Radiol Surg 2012;7:125–136.
Meyer CR, Boes JL, Kim B, Bland PH, Lecarpentier GL, Fowlkes JB, Roubidoux MA, Carson PL. Semiautomatic registration of

volumetric ultrasound scans. Ultrasound Med Biol 1999;25: 339–347.

Miga MI, Paulsen KD, Lemery JM, Eisner SD, Hartov A, Kennedy FE, Roberts DW. Model-updated image guidance: Initial clinical experiences with gravity-induced brain deformation. IEEE Trans Biomed Eng 1999;18:866–874.

Moskalik A, Carson PL, Meyer CR, Fowlkes JB, Rubin JM, Roubidoux MA. Registration of three-dimensional compound ultrasound scans of the breast for refraction and motion correction. Ultrasound Med Biol 1995;21:769–778.

Nabavi A, Black PM, Gering DT, Westin CF, Mehta V, Pergolizzi RS Jr, Ferrant M, Warfield SK, Hata N, Schwartz RB, Wells WM 3rd, Kikinis R, Jolesz FA. Serial intraoperative magnetic resonance imaging of brain shift. Neurosurgery 2001;48:787–797. discussion 97–98.

Narayanasamy G, LeCarpentier GL, Roubidoux M, Fowlkes JB, Schott AF, Carson PL. Spatial registration of temporally separated whole breast 3D ultrasound images. Med Phys 2009;36:4288–4300.

Neelin P. The MINC file format: From bytes to brains. NeuroImage 1998;7:S786.

Nimsky C, Fujita A, Ganslandt O, Von Keller B, Fahlbusch R. Volumetric assessment of glioma removal by intraoperative high-field magnetic resonance imaging. Neurosurgery 2004;55:358–370. discussion 70–71.

Nimsky C, Ganslandt O, Cerny S, Hastreiter P, Greiner G, Fahlbusch R. Quantification of, visualization of, and compensation for brain shift using intraoperative magnetic resonance imaging. Neurosurgery 2000;47:1070–1080.

Pennec X, Cachier P, Ayache N. Tracking brain deformation in time sequences of 3D US images. Pattern Recog Lett 2003;24:801–813.

Porter BC, Rubens DJ, Parker KJ. Three-dimensional frameless fusion of ultrasound liver volumes. Proc IEEE Ultrason Sympos 1999;2: 1577–1580.

Reinertsen I, Lindseth F, Unsgaard G, Collins DL. Clinical validation of vessel-based registration for correction of brain-shift. Med Image Anal 2007;11:673–684.

Risholm P, Samset E, Talos I-F, Wells WM 3rd. A non-rigid registration framework that accommodates resection and retraction. Inf Process Med Imaging 2009;21:447–458.

Roberts DW, Hartov A, Kennedy FE, Miga MI, Paulsen KD. Intraoperative brain shift and deformation: A quantitative analysis of cortical displacement in 28 cases. Neurosurgery 1998;43:749–758. discussion 58–60.

Roberts DW, Miga MI, Kennedy FE, Hartov A, Paulsen KD. Intraoperatively updated neuroimaging using brain modeling and sparse data. Neurosurgery 1999;45:1199–2207.

Roberts DW, Valdes PA, Harris BT, Fontaine K, Hartov A, Fan X, Ji S, Lollis S, Pogue BW, Leblond F, Wilson BC, Paulsen KD. Coregistered fluorescence-enhanced tumor resection of malignant glioma: Relationships between δ-aminolevulinic acid–induced protoporphyrin IX fluorescence, magnetic resonance imaging enhancement, and neuropathological parameters. J Neurosurg 2011;114:595–603.

Rohling RN, Gee AH, Berman L. Three-dimensional spatial compounding of ultrasound images. Med Image Anal 1997;1:177–193.

Rohling RN, Gee AH, Berman L. Automatic registration of 3-D ultrasound images. Ultrasound Med Biol 1998;24:841–854.

Rygh O, Selbekk T, Torp S, Lydersen S, Hernes T, Unsgaard G. Comparison of navigated 3D ultrasound findings with histopathology in subsequent phases of glioblastoma resection. Acta Neurochirurgica 2008;150:1033–1042.

Shekhar R, Zagrodsky V. Mutual information-based rigid and nonrigid registration of ultrasound volumes. IEEE Trans Med Imaging 2002;21:9–22.

Shekhar R, Zagrodsky V, Garcia MJ, Thomas JD. Registration of real-time 3-D ultrasound images of the heart for novel 3-D stress echocardiography. IEEE Trans Med Imaging 2004;23:1141–1149.

Solberg OV, Lindseth F, Torp H, Blake RE. Nagelhus Hernes TA. Freehand 3D ultrasound reconstruction algorithms: A review. Ultrasound Med Biol 2007;33:991–1009.

Stummer W, Pichlmeier U, Meinel T, Wiestler OD, Zanella F, Reulen HJ. Fluorescence-guided surgery with 5-aminolevulinic acid for resection of malignant glioma: A randomised controlled multicentre phase III trial. Lancet Oncol 2006;7:392–401.

Stupp R, Hegi ME, Mason WP, van den Bent MJ, Taphoorn MJB, Janzer RC, Ludwin SK. Effects of radiotherapy with concomitant and adjuvant temozolomide versus radiotherapy alone on survival in glioblastoma in a randomised phase III study: 5-year analysis of the EORTC-NCIC trial. LANONC 2009;10:459–466.

Tipnis SV, Nagarkar VV, Shestakova I, Gaysinskiy V, Entine G, Tornai MP, Stack BC Jr. Feasibility of a beta-gamma digital imaging probe for radioguided surgery. IEEE Transactions on Nuclear Science 2004;51:110–116.

Tirakotai W, Miller D, Heinze S, Benes L, Bertalanffy H, Sure U. A novel platform for image-guided ultrasound. Neurosurgery 2006;58:710–718. discussion 710–718.

Trantakis C, Tittgemeyer M, Schneider JP, Lindner D, Winkler D, Strauss G, Meixensberger J. Investigation of time-dependency of intracranial brain shift and its relation to the extent of tumor removal using intra-operative MRI. Neurol Res 2003;25:9–12.

Treece GM, Prager RW, Gee AH, Berman L. Correction of probe pressure artifacts in freehand 3D ultrasound. Med Image Anal 2002;6: 199–214.

Unsgaard G, Gronningsaeter A, Ommedal S, Nagelhus Hernes TA. Brain operations guided by real-time two-dimensional ultrasound: New possibilities as a result of improved image quality. Neurosurg Rev 2002a;25:68–72.

Unsgaard G, Ommedal S, Muller T, Gronningsaeter A, Nagelhus Hernes TA. Neuronavigation by intraoperative three-dimensional ultrasound: Initial experience during brain tumor resection. Neurosurgery 2002b;50:804–812. discussion, 12.

Unsgaard G, Selbekk T, Brostrup Muller T, Ommedal S, Torp SH, Myhr G, Bang J, Nagelhus Hernes TA. Ability of navigated 3D ultrasound to delineate gliomas and metastases: Comparison of image interpretations with histopathology. Acta Neurochir (Wien) 2005; 147:1259–1269. discussion, 69.

Wolfsberger S, Rössler K, Regatschnig R, Ungersböck K. Anatomical landmarks for image registration in frameless stereotactic neuronavigation. Neurosurg Rev 2002;25:68–72.

Woydt M, Krone A, Becker G, Schmidt K, Roggendorf W, Roosen K. Correlation of intra-operative ultrasound with histopathologic findings after tumour resection in supratentorial gliomas: A method to improve gross total tumour resection. Acta Neurochir (Wien) 1996;138:1391–1398.

Xiao G, Brady JM, Noble JA, Burcher M, English R. Nonrigid registration of 3-D free-hand ultrasound images of the breast. IEEE Trans Med Imaging 2002;21:405–412.

Yixun Liu, Chengjun Yao, Liang Fu Zhou. Nikos Chrisochoides: A point based non-rigid registration for tumor resection using IMRI. ISBI 2010;1217–1220.